

Controlling Morphology in Polymer–Fullerene Mixtures**

By Adam J. Moulé and Klaus Meerholz*

In the past several years, polymer–fullerene mixtures have been intensely studied for use in organic solar cells because they can be deposited from solution, are compatible with low-cost roll-to-roll fabrication technology, and have shown high power conversion efficiency (η), up to 4–5%.^[1–3] The best devices consist of a single bulk-heterojunction active layer, in which the polymer (donor) and fullerene (acceptor) are deposited from a common solvent. As the solvent dries the donor and acceptor components separate into domains. The final efficiency of the solar cell has been shown to be extremely sensitive to the size, composition, and crystallinity of the formed domains.^[4,5] Improvement of the morphology in devices fabricated with a mixture of [6,6]-phenyl C₆₁-butyric acid methyl ester (PCBM) and regioregular poly(3-hexylthiophene) (P3HT) has been achieved by using heat-treatment techniques^[2,6] and long-time solvent curing,^[1] with resulting record efficiencies. More recently, a method for increasing the crystallinity of the P3HT component has been introduced which involves filtering preformed nanofibers of P3HT out of solution and mixing the prepared nanofiber dispersion with PCBM to increase the efficiency of as-cast devices.^[7] Interestingly, the best device performance was achieved by mixing lower-molecular-weight (M_w) amorphous P3HT back into the solution to reduce the crystalline content of the active layer and, thereby, to increase connection between crystalline domains. Studies of the M_w impact on P3HT/PCBM solar cells have indicated that a large polydispersity and number-average molecular weight (M_n) over 19000 g mol⁻¹ leads to improved efficiency.^[8,9] Morphology studies of organic field-effect transistor (OFET) devices indicate that the increased M_w leads to better network formation between crystalline domains.^[10,11]

The morphology of these improved devices has been studied using transmission electron microscopy (TEM),^[12] grazing-angle X-ray diffraction (XRD),^[13,14] atomic force microscopy (AFM),^[10] scanning electron microscopy (SEM),^[15] NMR,^[16] and a variety of other optical^[14] and electrical techniques.^[17] The morphology studies give a picture of a device in which the P3HT forms aligned/crystalline domains, between which are amorphous segments of P3HT and PCBM.^[14] These domains form with larger size and crystallinity for higher heat-treatment temperatures^[18] and longer solvent soaking times.^[19,20] Depending on the fabrication and measurement techniques, the aligned domains of P3HT are depicted as fibers^[12] or as shapeless masses.^[14]

The majority of these studies do not, however, allow quantification of the percentage of the P3HT that is agglomerated/crystalline in the final device. Only by making use of the nanofiber filtration technique^[7] have the authors been given the ability to control the crystalline content of the P3HT in solution and in the final device. The disadvantages of this technique are the necessity of more complicated preparation, and filtered P3HT is restricted to a fibrous form that requires the addition of amorphous P3HT to provide connections between crystalline domains. We present here a simple method to determine the agglomerated–amorphous ratio of the P3HT and to control the degree of agglomeration/crystallinity of the P3HT in the final device by using a solvent mixing method and no further heat-treatment or prepreparation of the polymer.

The most obvious change that heat-treatment and solvent soaking yield on a P3HT:PCBM layers is the change in color.^[6,21,22] It has been widely reported that the P3HT absorption red-shifts and a series of vibronic peaks become visible at $\lambda \sim 600$ nm, 550 nm, and 510 nm.^[6,11] This red-shift has been assigned to increased planarization and stabilization of the P3HT chains that accompanies self-stacking of the polymer.^[10,14] The crystal structure for these self-stacking domains has been solved by using XRD and TEM, and shows a herringbone interconnection of the alkyl chains and an a -dimension stacking distance of 1.6 nm.^[14] The π – π chain stacking of the P3HT chains in crystallites has been measured to be 0.38 nm.^[13] The herringbone structure and planarization of the P3HT with heating has been confirmed using heteronuclear solid-state NMR measurements.^[16] The red-shift in the UV-vis spectrum occurs proportionally to the degree of agglomeration of the P3HT.^[7,23]

The pure amorphous electronic spectrum of P3HT or a mixture of P3HT and PCBM is simple to measure. A solution UV-vis spectrum can also be measured in the liquid state. If

[*] Prof. K. Meerholz, Dr. A. J. Moulé^[†]
Institute of Physical Chemistry
University of Cologne
Luxemburgerstr. 116, 50939 Köln (Germany)
E-mail: klaus.meerholz@uni-koeln.de

[†] Present address: University of California, Davis, Department of Chemical Engineering & Materials Science, 1 Shields Av., Davis, CA 95616, USA.

[**] We would like to acknowledge the Alexander von Humboldt foundation for the post-doctoral grant of A.M. We would also like to thank German Ministry of Science and Education (BMBF) for funding EKOS project (O3N2023D) and the ministry of Science and Innovation of Northrhine-Westfalia (Elena-project). We thank Tanja Tegeger for taking the SEM image. Supporting Information is available online from Wiley InterScience or from the authors.

the solvated polymer is titrated with an “unfriendly” solvent, a solvatochromic red-shift of the absorption spectrum occurs which is similar to the red-shift seen upon condensation into a film.^[24] Physically, the polymer forms nanoparticle aggregates in a stable mini-emulsion. This mini-emulsion effect has been used to make polymer solar cells and light-emitting diodes with highly controlled morphology.^[25–27] In the context of this study, the solvatochromic effect can be used to gain a quantitative comparison of the absorption features of liquid-phase and solid-phase P3HT.

A series of UV-vis spectra with different ratios of chlorobenzene (CIB) and *t*-butanol was recorded (see Supporting Information, Fig. S1a). It can be clearly seen that the amorphous P3HT spectrum red-shifts, and with high *t*-butanol concentration is completely composed of nanoparticles or aggregated P3HT. Measurement of the dispersion with high *t*-butanol concentration with dynamic light scattering indicates a narrow particle size distribution with diameter of about 55 nm (assuming a spherical particle). For comparison, a pure heat-treated P3HT thin-film spectrum cast from CIB is displayed. The aggregated and thin-film spectra are essentially identical (see Fig. S1b for direct comparison). Using this technique it is possible to get both the pure amorphous and pure aggregated spectrum, at identical mass-to-volume concentrations, and therefore to quantitatively compare the spectra. As has been previously shown, P3HT absorbs ~12% more strongly at the absorption maximum when aggregated.^[24]

As compared to the recent results given by Berson et al.,^[7] the solvent mixture used here produces 100% P3HT aggregated content, while they found 75% nanofiber content in *p*-xylene solutions. A method to produce P3HT nanofibers has been demonstrated by Ihn et al. and later Merlo et al. who described the spontaneous formation of nanofibers of P3HT in a *p*-xylene solution.^[28,29] The solution was, however, a mixture of P3HT nanofibers and amorphous P3HT that had to be filtered to obtain pure nanofibers. Our approach does not require filtering to obtain pure agglomerated P3HT, which is an important advantage for production of the organic photovoltaic (OPV) cells using solvent mixtures. By taking SEM images of the nanoparticles spin-cast from a dilute chloroform/methanol mixture onto indium tin oxide (ITO), it was possible to see that a network structure was formed with a minimum length scale of 20–30 nm (Fig. 1).

The principle of using an unfriendly/dipolar solvent is also interesting in order to control the aggregation of P3HT in mixed polymer–fullerene device layers. As has been shown by Zhang et al., a dopant solvent can have a large effect on the final morphology of a polymer–fullerene blend at very low concentrations if the dopant has a higher boiling point than the main solvent.^[30] We have found that adding 0.33–6.5% by volume of nitrobenzene (NtB) to a typical casting solvent, such as CIB, for P3HT:PCBM blend solar cells allows for a full control of the final device morphology. Specifically, the aggregated content of the P3HT can be adjusted from the as-cast CIB mixture value of 59% aggregated to 100% aggregated P3HT content. The solution itself does not change color, nor

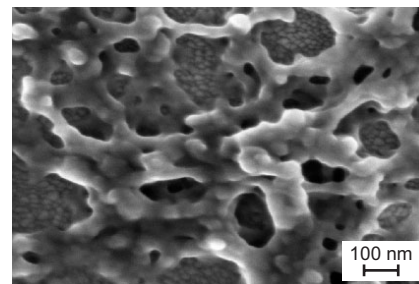


Figure 1: SEM image of P3HT spin cast from a dilute (0.1 mg mL^{-1}) solution of 1:1 chloroform/methanol onto an ITO substrate. The ITO is the grainy substance in the background. The P3HT forms into 3D networks because of rapid aggregation during drying.

is the aggregated content of the P3HT increased until the ratio of CIB:NtB in the spinning film is reduced to nearly pure NtB as a solvent. Depicted in Figure 2 are UV-vis spectra of as-cast thin-films with NtB doped into the casting solvent from 0% to 6.25% by volume. The peak at ~600 nm that is typically associated with agglomeration in P3HT grows with

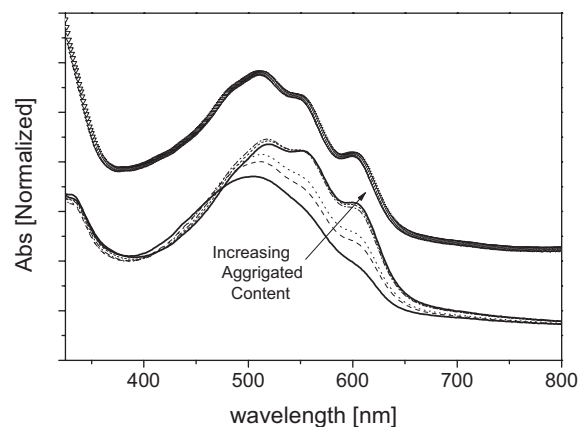


Figure 2. a) UV-vis spectra of 3:2 P3HT:PCBM as-cast PV devices with 0% (solid line), 0.33% (dashed line), 0.67% (dotted line), 1.6% (dashed-dotted line), 3.2% (short dashed line), and 6.3% (solid line) nitrobenzene added into the chlorobenzene solvent. Offset from the other spectra is the as-cast PV device from the *o*-xylene dispersion (triangles).

increased NtB content until, at 6.25% NtB concentration, the UV-vis spectrum can be fit using only the pure P3HT aggregated and PCBM spectra (Fig. S3). NtB itself has a strong visible absorption at ~400 nm. It is clear from the spectra that the NtB content in the as-cast film is below the detection limit.

For comparison, we fabricated devices with preformed nanofibers in a method similar to (and concurrent to) Berson et al.^[7] Here, P3HT is dissolved into *o*-xylene (OX) at high temperature and later stirred at room temperature for several days. The original red solution slowly changes color to black as the aggregated P3HT content increases. If the black solution is mixed with PCBM and used to make solar-cell layers,

the nanofibers are formed before the spin-casting process. As stated earlier, only a portion of the P3HT forms nanofibers in the OX (or p-xylene) solution.^[7] We were able to confirm that nanofibers are formed over time in OX by spincasting pure P3HT from the black solution and imaging the surface using tapping-mode AFM (Fig. S2).

The solid lines in Figure S1a represent the pure amorphous P3HT and pure aggregated P3HT at identical mass-to-volume concentrations. These spectra represent the pure components of P3HT in different configurations. When combined with the PCBM spectrum, it is now possible to quantitatively fit the ratio of amorphous–aggregated P3HT content (Fig. S3a) in a spin-cast device. The relative percentages of aggregated and amorphous P3HT in the devices is 35% and 25% for the device made from pure CIB and rapidly changes toward 60% and 0% when the content of NtB is increased (Fig. S3b). The PCBM was assumed to be 40% in all spectra. For reference, the film cast from OX-np dispersion has an 48%:12% aggregated–amorphous content. We were not able to measure the aggregated–amorphous ratio of P3HT using UV-vis in the OX solution because this ratio was both temperature- and concentration-dependent. Naturally, P3HT:PCBM films cast from other solvents and with other mixing ratios of P3HT:PCBM can be expected to have different ratios of aggregated–amorphous content.

In Figure 3 we show a comparison of the I – V curves of as-cast and heat-treated 3:2 P3HT:PCBM solar cells. A 3:2 ratio was chosen for these devices because previous studies in our group have shown that this ratio is optimal for 80 nm thick devices.^[31] The devices were cast from pure amorphous (recently heated) solutions of CIB (CIB-amorph) and OX (OX-amorph), as well as a CIB cast devices with 4.25% NtB content (CIB/NtB) and a device cast from a black OX dispersion

(OX-np). Interestingly, the devices cast from CIB-amorph and OX-amorph have identical properties and efficiency of ~1.2%. The increased aggregated content present in the OX-np device increases both the short-circuit current density (J_{sc}) and the fill factor (FF) of the devices and gives an efficiency of 3.28%, which is very similar to that reported by Berson et al.^[7] The fully aggregated CIB/NtB device shows the best efficiency with 3.94%. All of the devices have a thickness ~80 nm, as determined by UV-vis absorption and profilometry.

After measurement, each of the device types was heat-treated at 150–180 °C (see Fig. S4 for heat-treatment characteristics of all devices). The CIB-amorph and OX-amorph devices showed the largest improvement after heat-treatment at 150 °C for 15 min. The devices still show nearly identical I – V curves and efficiencies of 4.3%. It has been previously reported that spin-casting from CIB leads to vertical segregation of the P3HT and PCBM,^[32] while spin-casting from OX does not.^[33] Because our results show nearly identical behavior for amorphous CIB and OX cast devices for all heat-treatment temperatures, we conclude that either no or identical vertical segregation occurs for these solvents.

Comparison of the heat-treated CIB/NtB and OX-np devices also yields an interesting result (Fig. 3b). The CIB/NtB device maintains its high J_{sc} , but the open-circuit voltage (V_{oc}) improves to 0.66 V. The best efficiency is also ~4.3% for 180 °C heat-treatment. The J_{sc} of the OX-np device also improves with heat-treatment, but never reaches the value of the other heat-treated devices. In addition, both the FF and V_{oc} of the OX-np dispersion device are reduced with heat-treatment, so the best efficiency remains 3.3% with 180 °C heat-treatment. Since the nanofibers in the OX-np dispersion are formed before spin-coating, it is most likely that no PCBM is able to penetrate into the P3HT fibers after casting. We believe that the J_{sc} is reduced in these devices because some of the excitons formed in the P3HT domains are too far from a donor/acceptor interface to undergo charge separation. By comparison, aggregated P3HT networks are formed as the CIB/NtB solution evaporates during the spin-coating process. It is most likely that some PCBM remains in the domains to facilitate charge transfer and that the 3D network of agglomerated P3HT has superior charge-transport properties.

This result shows that the preparation of nearly 4% efficient solar cells is possible without heat-treatment, solvent-soaking, or any other special preparation of the components. The control of morphology by the addition of an unfriendly dopant solvent allows the improvement of all of the I – V characteristics except the V_{oc} . The V_{oc} of the heat-treated samples improves to 0.66 V. We believe that the improvement of the V_{oc} is probably due to better wetting by the metal electrode or a structural change at the PEDOT:PSS/active layer interface.

The change in the ratio of amorphous–aggregated P3HT that accompanies the addition of NtB to the spin-coating solution results in a morphology change. Fitting of the absorption spectrum with the pure PCBM, P3HT aggregated, and P3HT amorphous spectra gives a quantitative measure of the P3HT

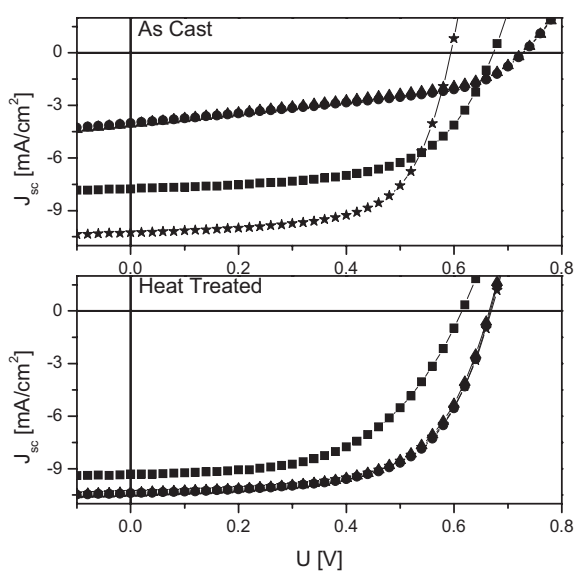


Figure 3. I – V curves of as-cast (upper) and heat-treated (lower) 3:2 P3HT:PCBM devices. The devices were cast from CIB-amorph (triangles), OX-amorph (circles), OX-np (squares), and CIB/NtB (stars).

phase behavior but does not give a morphological picture of what the effect of the NtB additive yields. In previous reports detailing the effects of heat-treatment and long-time solvent soaking on the improvement of P3HT/PCBM solar cells, an increase in surface roughness and an increase in the phase separation was documented using AFM.^[1,2] In Figure 4, we show that the surface roughness increases and that the average domain size also increases with increased aggregated pro-

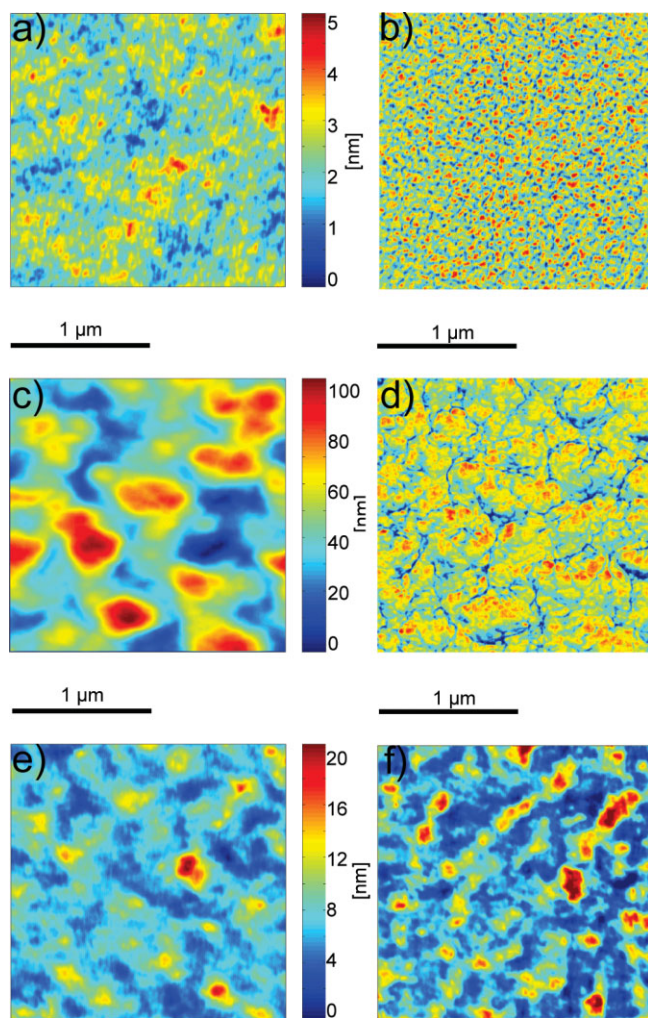


Figure 4. Tapping mode AFM topography and phase images of as-cast OPV devices cast from a,b) chlorobenzene, c,d) chlorobenzene with 4.25% nitrobenzene added, and e,f) o-xylene with preformed P3HT nanofiber content). The color code used in (b), (d), and (f) is identical.

portion of P3HT. Figure 4 compares as-cast CIB-amorph, CIB/NtB, and OX-np samples. The topography images show striking differences. The root mean square (rms) roughness of the CIB/NtB sample is an order of magnitude larger than for the CIB-amorph sample. Considering that the average sample thickness (as measured by UV-vis, profilometry, and AFM of scratched surface) in each case was ~80 nm, the CIB/NtB sample must be less than 35 nm thick in some locations and more

than 125 nm thick in others. With this large, pre-electrode- evaporation roughness we would expect that the CIB/NtB sample would suffer electrical contact problems at the metal cathode. The *I*-*V* curves in Figure 3 indicate, however, that the active layer has excellent electrical contact, as indicated by the high FF. We also show an AFM image of an as-cast OX-np sample. The surface roughness has an intermediate roughness between the CIB-amorph and CIB/NtB samples. No nanofiber structures can be seen in any of these images, though we know that nanofibers are incorporated into the OX-np cast layer by comparison as-cast films of pure P3HT (Fig. S2).

The apparent average domain size, as measured by an AFM phase image, increases greatly in both the CIB/NtB and OX-np samples. The interpretation of the phase information has, however, been greatly complicated by the new picture of P3HT in an aggregated and amorphous configuration. The phase image generally gives a picture of the change in surface “hardness”, in which a two-component mixture, such as a polymer–fullerene mixture, can be interpreted as showing fullerene-rich and fullerene-poor domains.^[34] With the presence of P3HT in amorphous and aggregated configurations, this is effectively a multicomponent system (amorphous P3HT rich and poor in PCBM, and aggregated P3HT rich and poor in PCBM).

We show, using UV-vis measurements (Fig. S3a and b), that the as-cast CIB sample has a 35.4%:24.6% ratio of aggregated–amorphous P3HT content. Grazing-angle XRD measurements have shown no crystalline content in as-cast films of 1:2 P3HT:PCBM using CIB and chloroform as casting solvents.^[13,14] The same study shows that as-cast pure P3HT films do have crystalline content.^[13] However, high-resolution TEM measurements have shown the presence of nanocrystalline domains even in untreated 1:2 P3HT:PCBM samples using o-dichlorobenzene as a casting solvent.^[12] The CIB-amorph phase image (Fig. 4b) shows a very fine domain separation (< 50 nm) that is consistent with the formation of nanocrystalline domains. Even though the layers were cast from CLB and not heat treated, we believe that some crystalline P3HT forms due to the high P3HT content in the layer.

From the UV-vis measurements, we expect the CIB/NtB sample to have ~99% aggregated P3HT content. The apparent domain size is also much larger to an average of over 100 nm in size. Because essentially all of the P3HT is aggregated, we believe that the phase image can be interpreted as P3HT-rich domains (red–yellow) and PCBM-rich (cyan–blue) veins. This assignment is based on the idea that during spin-coating, aggregated P3HT-rich networks form with rounded domains and PCBM-rich veins are left between. Owing to the 3:2 P3HT:PCBM mixing ratio, there is a larger P3HT content in the layer. The large P3HT-rich domains are seen as red–yellow in Figure 4d with comparatively smaller PCBM-rich veins. The exciton diffusion length in a similar conjugated polymer, OC₁C₁₀-PPV, has been measured to be ~5 nm.^[35] Considering the high efficiency of the CIB/NtB device, there

must still be enough PCBM in the predominately P3HT networks to ensure charge separation and transport out of the domains.

In the as-cast OX-np sample, we calculated a ~80% aggregated P3HT content. Some of the aggregated P3HT domains were formed in solution and, therefore, cannot contain PCBM. The phase image shows the greatest phase separation of the three samples with domains of over 300 nm. The as-cast and heat-treated devices shown in Figure 3 have reduced J_{sc} values with respect to the CIB/NtB and heat-treated OX-amorph and CIB-amorph samples. We take this as proof that the degree of separation in the OX-np samples is too high and that some of the excitons formed do not separate into charges because they are too far from a donor/acceptor interface. After heat-treatment, the CIB/NtB and OX-np samples show very little change in the topography and phase AFM images (data not shown). The CIB-amorph sample shows increased surface roughness and increased domain size, as has been previously published.^[2]

In conclusion, we have shown that the P3HT component of the P3HT/PCBM solar cells mixture is found in both aggregated and amorphous configurations. The ratio of the P3HT in the amorphous and aggregated phases can be controlled both in solution and in spin-cast films by adding a dipolar solvent that causes the P3HT to aggregate into nanoparticles or nanodomains, respectively. Reference to previous studies indicates that these nanoparticles/nanodomains are at least partially crystalline. Evidence for this change between an amorphous and aggregated phase is given by the shape change of the UV-vis spectrum and AFM and SEM images of the formed nanostructures. We were able to use P3HT dissolved in a "friendly" solvent to measure the amorphous absorption. When a dipolar, but miscible second solvent is added to the solution, the P3HT forms nanoparticles that yield a fully aggregated or solid-state spectrum. In this way the amorphous and aggregated spectra could be compared quantitatively in the liquid phase.

Using the principle of a dipolar additive to control aggregation, we show that we can fabricate P3HT/PCBM solar cells with between < 59% and 100% aggregated P3HT by adding nitrobenzene to the solvent mixture. Layers spin-cast with over 4% NtB content have ~100% aggregated P3HT content. The addition of the NtB causes the formation of aggregated P3HT networks during the drying process so that devices with nearly 4% power efficiency under AM1.5 illumination can be fabricated with no pre- or post-treatment steps, such as filtration, heat-treatment, or solvent soaking. After heat-treatment, devices cast from CIB-amorph, OX-amorph and CIB/NtB solutions have nearly identical $I-V$ characteristics. The J_{sc} does not change for the CIB/NtB sample with heat-treatment but the V_{oc} increases, which leads to a power efficiency of ~4.3%.

Comparisons were also made with devices that incorporate preformed P3HT fibers that are cast from OX. The increase in the aggregated content improves the device quality for as-cast devices but is limited after heat-treatment because of ex-

clusion of PCBM from the aggregated P3HT domains. These observations are supported by AFM tapping-mode phase images that show larger domain size than for CIB-amorph and CIB/NtB samples. There is no question that increasing the aggregated/crystalline content of the P3HT increases the device efficiency. What we have shown here is that not only must the P3HT domains be crystalline, they must also be connected into a network for charge transport and they must also be formed during the spin coating process so that the PCBM is not completely excluded from the aggregated network. Exclusion of PCBM leads to reduced charge separation and reduced efficiency.

Experimental

All of the solar cells in this work were prepared on commercial ITO-coated glass with layer thickness ~140 nm and 15 O sheet resistance (Merck). The ITO was etched with acid and subsequently cleaned using chloroform, acetone, Mucosal detergent, and deionized water in an ultrasonic bath. The cleaned ITO samples were exposed to ozone for 10 min and immediately spin coated with 31 nm of PEDOT:PSS (Baytron P AL 4083, HC Stark). The PEDOT:PSS-coated samples were heat-treated at 110 °C for 3 min and then moved to a N₂ glove box for the remainder of the fabrication and measurement. The CIB and OX polymer solutions were stirred overnight at 60 °C before spin coating to ensure that the polymer had been completely dissolved. The active layer of the solar cells was spin-coated from a 3:2 mixture of P3HT (Aldrich, reported regioregularity > 98.5%) and PCBM (Nano-C), because this ratio was determined to be best for a 80 nm active layer thickness.^[31] The P3HT was cleaned twice prior to making the final solution by dissolving the polymer into CIB and crashing the polymer into a 7:1 methanol-water solution dropwise, followed by filtration. After spin-coating of the active layer, the samples were moved to a high vacuum chamber (~10⁻⁶ mbar), where an electrode of 5 nm Ca and 150 nm Ag was vapor-deposited through a mask, leaving 7 solar cells with an active area of 0.0785 cm². After metal deposition, the samples were either directly measured or tempered for 10 min at various temperatures (see Fig. S4) in N₂ atmosphere. OX-np dispersions were made by heating over night and then continued stirring at room temperature for several days (2–14) before spin-coating. We did not conduct a systematic study to determine the rate of nanofiber formation.

The $I-V$ curves of the samples were measured using a Keithley 2425 source measurement unit in an N₂ glove box. AM1.5 illumination at 100 mW cm⁻² was provided by a filtered Xe lamp and calibrated by using a calibrated solar cell from the Fraunhofer institute for solar research (Freiburg, Germany). Sample thickness was determined using a Dektak surface profiler that was calibrated to a Si-SiO₂ ellipsometry standard. Sample thicknesses were double-checked using AFM. AFM measurements were performed on a SIS pico-station mode microscope in tapping mode. All images were acquired with 512 × 512 points and a measuring speed of 0.9 s line⁻¹. UV-vis measurements were performed on a Varian Cary spectrometer. Dynamic light-scattering measurements of particle size in solution were performed with a Malvern Zetasizer device. The SEM image was measured using a field emission Zeiss Supra 40VP with a 2 kV acceleration voltage and an in-line detector.

Received: June 25, 2007

Revised: August 2, 2007

Published online: December 20, 2007

[1] G. Li, V. Shrotriya, J. Huang, Y. Yao, T. Moriarty, K. Emery, Y. Yang, *Nat. Mater.* **2005**, *4*, 864.

- [2] W. Ma, C. Yang, X. Gong, K. Lee, A. J. Heeger, *Adv. Funct. Mater.* **2005**, *15*, 1617.
- [3] M. Reyes-Reyes, K. Kim, D. L. Carroll, *Appl. Phys. Lett.* **2005**, *87*, 083506.
- [4] H. Hoppe, N. S. Sariciftci, *J. Mater. Chem.* **2006**, *16*, 45.
- [5] J. J. M. Halls, A. C. Arias, J. D. MacKenzie, W. S. Wu, M. Inbasekaran, E. P. Woo, R. H. Friend, *Adv. Mater.* **2000**, *12*, 498.
- [6] F. Padinger, R. S. Rittberger, N. S. Sariciftci, *Adv. Funct. Mater.* **2003**, *13*, 85.
- [7] S. Berson, R. De Bettignies, S. Bailly, S. Guillerez, *Adv. Funct. Mater.* **2007**, *17*, 1377.
- [8] R. C. Hiorns, R. De Bettignies, J. Leroy, S. Bailly, M. Firon, C. Sentein, A. Khoukh, H. Preud'homme, C. Dagron-Lartigau, *Adv. Funct. Mater.* **2006**, *16*, 2263.
- [9] P. Schilinsky, U. Asawapirom, U. Scherf, M. Biele, C. J. Brabec, *Chem. Mater.* **2005**, *17*, 2175.
- [10] R. J. Kline, M. D. McGehee, E. N. Kadnikova, J. S. Liu, J. M. J. Frechet, M. F. Toney, *Macromolecules* **2005**, *38*, 3312.
- [11] A. Zen, J. Pflaum, S. Hirschmann, W. Zhuang, F. Jaiser, U. Asawapirom, J. P. Rabe, U. Scherf, D. Neher, *Adv. Funct. Mater.* **2004**, *14*, 757.
- [12] X. N. Yang, J. Loos, S. C. Veenstra, W. J. H. Verhees, M. M. Wienk, J. M. Kroon, M. A. J. Michels, R. A. J. Janssen, *Nano Lett.* **2005**, *5*, 579.
- [13] P. Vanlaeke, A. Swinnen, I. Haeldermans, G. Vanhoyland, T. Aernouts, D. Cheyns, C. Deibel, J. D'Haen, P. Heremans, J. Poortmans, J. V. Manca, *Sol. Energy Mater. Sol. Cells* **2006**, *90*, 2150.
- [14] T. Erb, U. Zhokhavets, G. Gobsch, S. Raleva, B. Stuhn, P. Schilinsky, C. Waldauf, C. J. Brabec, *Adv. Funct. Mater.* **2005**, *15*, 1193.
- [15] H. Hoppe, M. Niggemann, C. Winder, J. Kraut, R. Hiesgen, A. Hinsch, D. Meissner, N. S. Sariciftci, *Adv. Funct. Mater.* **2004**, *14*, 1005.
- [16] C. Y. Yang, J. G. Hu, A. J. Heeger, *J. Am. Chem. Soc.* **2006**, *128*, 12007.
- [17] V. D. Mihailetschi, H. X. Xie, B. de Boer, L. M. Popescu, J. C. Hummelen, P. W. M. Blom, L. J. A. Koster, *Appl. Phys. Lett.* **2006**, *89*, 012107.
- [18] G. Li, V. Shrotriya, Y. Yao, Y. Yang, *J. Appl. Phys.* **2005**, *98*, 043704.
- [19] J. S. Huang, G. Li, Y. Yang, *Appl. Phys. Lett.* **2005**, *87*, 112105.
- [20] K. Inoue, R. Ulbricht, P. C. Madakasira, W. M. Sampson, S. Lee, J. Gutierrez, J. Ferraris, A. A. Zakhidov, *Synth. Met.* **2005**, *154*, 41.
- [21] T. J. Savenije, J. E. Kroeze, X. N. Yang, J. Loos, *Adv. Funct. Mater.* **2005**, *15*, 1260.
- [22] N. Camaioni, G. Ridolfi, G. Casalbore-Miceli, G. Possamai, M. Maggini, *Adv. Mater.* **2002**, *14*, 1735.
- [23] P. J. Brown, D. S. Thomas, A. Kohler, J. S. Wilson, J. S. Kim, C. M. Ramsdale, H. Sirringhaus, R. H. Friend, *Phys. Rev. B* **2003**, *67*, 064203.
- [24] M. M. Bouman, E. E. Havinga, R. A. J. Janssen, E. W. Meijer, *Mol. Cryst. Liq. Cryst. Sci. Technol., Sect. A* **1994**, *256*, 439.
- [25] T. Kietzke, D. Neher, M. Kumke, R. Montenegro, K. Landfester, U. Scherf, *Macromolecules* **2004**, *37*, 4882.
- [26] T. Kietzke, D. Neher, K. Landfester, R. Montenegro, R. Guntner, U. Scherf, *Nat. Mater.* **2003**, *2*, 408.
- [27] T. Piok, S. Gamerith, C. Gadermaier, H. Plank, F. P. Wenzl, S. Patil, R. Montenegro, T. Kietzke, D. Neher, U. Scherf, K. Landfester, E. J. W. List, *Adv. Mater.* **2003**, *15*, 800.
- [28] J. A. Merlo, C. D. Frisbie, *J. Polym. Sci. B* **2003**, *41*, 2674.
- [29] K. J. Ihn, J. Moulton, P. Smith, *J. Polym. Sci. B* **1993**, *31*, 735.
- [30] F. L. Zhang, K. G. Jespersen, C. Bjorstrom, M. Svensson, M. R. Andersson, V. Sundstrom, K. Magnusson, E. Moons, A. Yartsev, O. Inganäs, *Adv. Funct. Mater.* **2006**, *16*, 667.
- [31] A. J. Moulé, J. B. Bonekamp, K. Meerholz, *J. Appl. Phys.* **2006**, *100*, 094503.
- [32] Y. Kim, S. A. Choulis, J. Nelson, D. D. C. Bradley, S. Cook, J. R. Durrant, *Appl. Phys. Lett.* **2005**, *86*, 063502.
- [33] C. Waldauf, M. Morana, P. Denk, P. Schilinsky, K. Coakley, S. A. Choulis, C. J. Brabec, *Appl. Phys. Lett.* **2006**, *89*, 233517.
- [34] J. K. J. van Duren, X. N. Yang, J. Loos, C. W. T. Bulle-Lieuwma, A. B. Sieval, J. C. Hummelen, R. A. J. Janssen, *Adv. Funct. Mater.* **2004**, *14*, 425.
- [35] D. E. Markov, E. Amsterdam, P. W. M. Blom, A. B. Sieval, J. C. Hummelen, *J. Phys. Chem. A* **2005**, *109*, 5266.